This article has been accepted for publication in a future issue of this journal, but has not been fully edited. Content may change prior to final publication.
Citation information: DOI 10.1109/JIOT.2025.3565925, IEEE Internet of Things Journal

Performance Analysis of Terahertz Communication Systems with RSMA and Hardware Impairments

Xiangbin Yu, *Senior Member, IEEE*, Yue Zhou, Yun Rui, *Senior Member, IEEE*, Kezhi Wang, *Senior Member, IEEE*, Xiaoyu Dang, *Member, IEEE*

***Abstract*—Terahertz (THz) communication has received much attention recently for its large bandwidth availability, high data-rate transmission and alleviating the spectrum shortage, and it can meet the requirements of Internet of Things with large system capacity and networking capability. In this paper, the performance of multi-antenna THz communication systems with rate-splitting multiple access (RSMA) under the hardware impairments and imperfect successive interference cancelation (SIC) are investigated, where the THz channel is modeled as a composite fading channel including the molecular absorption effects, misalignment fading and small-scale $\alpha-\mu$ fading. Taking the hardware impairments and imperfect SIC into account, the probability density function and cumulative distribution function of the effective channel gain are derived. A joint zero-forcing and maximum ratio transmission beamforming design is employed to eliminate the interference among devices. Then, with the performance analysis, the closed-form outage probability (OP) and diversity gain of the system are respectively deduced. By minimizing the OP, a closed-form power allocation (PA) scheme is proposed to adjust the PA coefficients between the common stream and private streams, and resultant lower OP is attained. Moreover, the closed-form expression of the ergodic sum rate (ESR) is derived by means of Fox-H function and the Meijer-G function. With this ESR expression, the asymptotic ESR at high signal to noise ratio (SNR) is also provided to gain further insights. Furthermore, a simple upper bound of the ESR is derived for performance evaluation based on the Jensen's inequality. Simulation results show that the theoretical analysis is effective, and the proposed PA scheme can obtain lower OP. Besides, the impact of different system and fading parameters on the performance are also analyzed.**

***Index Terms*—THz communication, rate-splitting multiple access, outage probability, ergodic rate, power allocation, hardware impairment.**

I. Introduction

As one of the key technologies meeting the requirements for 6G, Terahertz (THz) communication is gradually becoming the focus of both scientific research and industry due to its unique technical principles and broad application prospects, and it can provide large bandwidth and high-speed transmission rate to support prospective 6G scenarios from space to ground and from macro-scale to nano-scale [1]. Specifically, this technology transmits information by modulating electromagnetic waves in the THz band, utilizing its abundant bandwidth resources. Theoretically, it can achieve data transmission rates of up to several Gbps or even tens of Gbps, providing strong support for high-speed data transmission. Thus, it can meet the requirements of large system capacity and networking capabilities for Internet of Things (IoT) [2] [3]. Meanwhile, due to the significant propagation attenuation of THz waves in the air, it limits their transmission distance, but also brings high communication security as the signals are not easily intercepted over long distances. The application fields of THz communication technology will be extensive and profound [4].

On the other hand, as a promising multiple access technique in future 6G communication, rate-splitting multiple access (RSMA) has high spectrum efficiency, enables dynamic resource allocation at the physical layer, and allows multiple users to share the same communication channel while maintaining their respective data transmission rates. The core idea of RSMA is to split the transmission rate of the channel into multiple sub-rates, each corresponding to a user's data stream, thereby enabling multiple users to access the same channel simultaneously without interference. The advantages of RSMA lie in its flexibility and high efficiency. Compared to traditional multiple access technologies, RSMA can dynamically adjust each user's transmission rate based on the users' demands and channel conditions, optimizing spectrum utilization. Furthermore, RSMA can reduce the channel interference and improve the system stability and reliability [5]. According to the above analysis, considering the high bandwidth and low latency characteristics of THz communication, as well as high resources utilization and multiuser support capabilities of RSMA, the THz communication and RSMA can be effectively combined to improve the overall system performance by utilizing their complementary advantages. Moreover, their combination can meet the requirements of high bandwidth, low latency, multi-user access and scalability of the communication systems, and thus provide effective support for the development and application of IoT networks.

A. Related Work

1) Performance of RSMA communication systems: There have been some studies on the performance analysis of RSMA and/or THz communication systems. For RSMA communication systems, the outage performance of a RSMA-assisted semi-grant-free transmission system was studied in [6]. In conjunction with cognitive radio techniques, the transmit power allocation, target rate allocation and successive interference

This work was supported in part by the Natural Science Foundation of China (62471228, 62031017).

X.Yu, Y. Zhou and X. Dang are with College of Electronic and Information Engineering, Nanjing University of Aeronautics and Astronautics, Nanjing, China. Y. Rui is with School of Communication and Electronic Engineering, East China Normal University, Shanghai, China. K.Wang is with Department of Computer Science, Brunel University London, Uxbridge, Middlesex, UB8 3PH, United Kingdom. X. Dang is also with Space Information Research Institute, Hangzhou Dianzi University.

Citation information: DOI 10.1109/JIOT.2025.3565925, IEEE Internet of Things Journal

cancelation decoding order of admitted grant free users (GFUs) were jointly optimized to maximize the reachable rate of GFUs. Meanwhile, theoretical and asymptotic expressions for the outage probability (OP) of the GFUs were derived. The authors in [7] investigated the performance of RSMA in finite block length uplink communication system, and the results showed that RSMA can outperform non-orthogonal multiple access scheme in terms of throughput and error probability performance. The outage performance of the millimeter-Wave (mmWave) RSMA multiple-input-single-output system with a fixed-located user and a randomly-located user was investigated in [8], where two beamforming (BF) schemes were proposed to improve the reliability of the mmWave RSMA system.

2) Performance of THz communication systems: For the THz communication systems, the performance analysis has also been addressed. In [9], the THz channels model in the presence of pointing errors and small-scale fading was presented, where the theoretical expressions for OP, average channel capacity and symbol error rate (SER) were derived along with the impact on system performance. The authors in [10] studied the performance of THz communication systems with hardware impairments and derived theoretical average signal-to-noise ratio (SNR), ergodic capacity and average bit error rate (BER) for the performance evaluation. In [11], the outage performance of the THz communication system with antenna misalignment and phase noise (PHN) was addressed, where the adverse effects of antenna misalignment and PHN on the system performance were revealed. In [12], the THz communication in the presence of pointing error and random foggy conditions was considered. By the performance analysis, the theoretical and approximate expressions for the SER and ergodic channel capacity were derived, respectively. In [13], the channel characterization and capacity analysis for THz communication-enabled smart rail mobility was addressed. In terms of the realistic channel information, the channel capacity of THz communication was derived, and the results provided valuable insights for the system evaluation in THz communication-enabled smart rail mobility. In [14], a Terahertz/free space optical (THz/FSO) wireless transmission system was presented, and the theoretical expressions for OP, BER and average channel capacity were deduced for the performance evaluation. Due to the high propagation attenuation of THz waves in air, it is important to combine with other techniques to enhance the THz communication performance. In [15], the performance of a dual-hop relay THz communication system considering fading and pointing error is investigated, where the OP, BER and average channel capacity of the system were analyzed. The results indicated that the dual-hop relay scheme has better performance than the single THz link. The performance of data collection from an IoT network located in hard-to-reach areas was analyzed considering the hybrid mmWave/FSO/THz backhaul link in [16], and the OP and BER performances of the integrated link that comprises the IoT and backhaul link were evaluated. In [17], the performance of an active reconfigurable intelligent surface-assisted mixed radio frequency-terahertz relaying system was investigated considering the amplify-and-forward and decode-and-forward protocols for the relay, and the theoretical OP, average BER, and average channel capacity were deduced for the evaluation.

3) Performance of RSMA-aided THz communication systems: The above works did not consider the superiority of RSMA. For this reason, the authors in [18] provided a unified framework analysis of the RSMA-aided THz (RSMA-THz) system based on a spherical stochastic model and proposed a precoding weighted design method with zero-forcing and maximum ratio transmission for suppressing the interference. Also, the user's OP and the throughput of the system were deduced, where the complex Gaussian fading was used to model the small-scale fading of the THz composite channels, and the practical misalignment fading was neglected for convenient analysis. Besides, by using the salp swarm algorithm, the authors in [19] optimized the energy efficiency of an intelligent reflective surface-assisted multiuser RSMA-THz system, and the resultant system performance was effectively increased.

B. Motivation, Contribution, and Organization

According to the analysis above, the performance analysis for RSMA/THz communication systems is well addressed, but the related work on the RSMA-THz is less studied, especially in the presence of the hardware impairment (HWI) or imperfect successive interference cancelation (SIC). To the best of our knowledge, the performance of RSMA-THz systems with the HWI and imperfect SIC is not studied. In practice, the hardware impairments will be unavoidable due to the IQ imbalance, nonlinear amplification, phase noise, etc [20] [21] [10]. Besides, the SIC may be incomplete because of the channel fading or the improper resource allocation [22] [23]. Hence, it is of practical significance to take HWIs and imperfect SIC into account when analyzing the performance of RSMA-THz communication systems. Furthermore, the more general composite THz channel including small-scale $\alpha-\mu$ fading, misalignment fading and molecular absorption effects is not considered.

Based on the above literature survey, we will investigate the performance of multi-antenna RSMA-THz communication system with the HWIs and imperfect SIC, and model the THz fading channel by using the composite channel with $\alpha-\mu$ fading and misalignment fading as well as molecular absorption effects in practice. Considering the actual HWIs at the transmitter and the receiver as well as imperfect SIC, we derive the closed-form expression of the OP and the corresponding power allocation (PA), and further derive the ergodic sum rate (ESR) of the system and its asymptotic expression as well as upper bound for the performance analysis and evaluation. The main contributions of this paper are summarized as follows:

1) By considering the molecular absorption effects, misalignment fading and small-scale $\alpha-\mu$ fading in practice for THz channel model, we investigate the OP and ergodic rate performance of multi-antenna THz communication systems with RSMA in the presence of transceiver hardware impairment and imperfect SIC. The probability density function (PDF) and the cumulative distribution function (CDF) of effective channel gains are firstly derived for the performance analysis. As a result, closed-form expressions can be attained.

This article has been accepted for publication in a future issue of this journal, but has not been fully edited. Content may change prior to final publication.
Citation information: DOI 10.1109/JIOT.2025.3565925, IEEE Internet of Things Journal

2) With the results above, we analyze the OP of the system for the performance evaluation and optimization. Correspondingly, the closed-form OP expression is deduced. Based on this, the asymptotic OP at high SNR is also derived, and resultant diversity gain of the system is attained. Besides, the PA coefficients of common stream and private streams are designed by minimizing the system OP. As a result, the closed-form PA scheme is attained. With this PA scheme, the system can achieve lower OP than the conventional fixed PA scheme.

3) By means of Fox-H and the Meijer-G functions, we derive the closed-form expressions of the ESR for the performance evaluation. With these expressions, the asymptotic ESR at high SNR is provided to gain the insights. By using the Jensen's inequality, the upper bound of ESR is also derived for simplifying the calculation of ESR. Besides, when the small-scale fading follows Nakagami-m fading (which corresponds to $\alpha = 2$), the closed-form ESR and its upper bound are also derived for performance analysis. The derived theoretical OP and ESR expressions can include the ones under perfect transceiver hardware and perfect SIC as special cases.

4) Simulation results show that the theoretical analysis ia valid, and can agree the corresponding simulation well. Moreover, with the proposed PA scheme, a lower OP can be attained, as expected. Furthermore, the impact of antenna number, small-scale fading parameters, misalignment fading parameter, hardware impairment level, and interference transfer factor on the system performance are also analyzed for the system optimization and design.

The remainder of the paper is organized as follows. Section II presents the system model for the RSMA-THz communication system. In Section III, the system OP is analyzed and derived, and an adaptive PA scheme is developed to minimize the OP. Section IV analyzes the ESR of the system, where the ESR and its upper bound are deduced. Simulation results are offered in Section V, and the main conclusions are drawn in Section VI.

Notations: matrix and vector are represented by using the boldface upper and lower case symbols, respectively. $(\cdot)^H$ denotes conjugate transpose. $\|\cdot\|$ and $|\cdot|$ stand for the 2-norm and absolute value, respectively. $CN\left(a,b\right)$ denotes complex Gaussian distribution, whose expectation is a and variance is b. $\mathbb{E}\left[\cdot\right]$ and $\mathrm{diag}(\cdot)$ represent the expectation and diagonalization operator, respectively

II. System model

As illustrated in Fig. 1, we consider a multi-antenna RSMA-THz communication system, including a base station (BS) with N antennas and K user devices (UDs) with single antenna. The BS transmits the information to all UDs via the RSMA scheme. The channel matrix is denoted as $\mathbf{H} = [\mathbf{h}_1, ..., \mathbf{h}_K] \in \mathbb{C}^{N\times K}$, where $\mathbf{h}_k \in \mathbb{C}^{N\times 1}$ is the channel vector from BS to device k (i.e. U_k). For multi-device RSMA-THz systems, there are K messages $\{W_k, 1 \le k \le K\}$ sent to K devices $\{U_k, 1 \le k \le K\}$. The message W_k of device k is divided into two parts, namely the common part $W_{c,k}$ and the private part $W_{p,k}$, where $W_{c,k}$ is encoded into the common stream s_c and $W_{p,k}$ is encoded into the private stream s_k separately, which satisfy $\mathbb{E}\left[|s_c|^2\right] = \mathbb{E}\left[|s_k|^2\right] = 1$. The common stream s_c can be decoded by all UDs, while the private stream s_k can only be decoded by the corresponding device U_k.

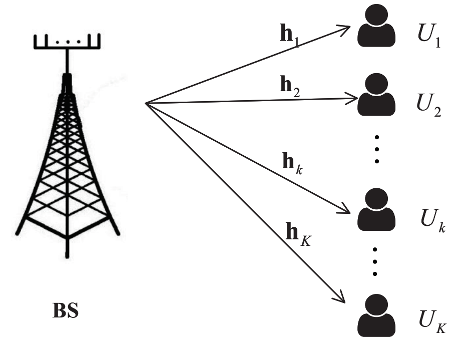

Fig. 1. RSMA-THz system model.

According to the RSMA scheme, the transmit signal after beamforming at BS can be given by

$$\mathbf{s} = \sqrt{a_c P_s}\mathbf{w}_c s_c + \textstyle\sum_{k=1}^{K} \sqrt{a_k P_s}\mathbf{w}_k s_k, \tag{1}$$

where P_s is is the transmit power of BS, a_c is the PA coefficients of the common stream and a_k is the PA coefficients of the private stream sent to the U_k, satisfying $a_c + \sum_{k=1}^{K} a_k = 1$. $\mathbf{w}_c \in \mathbb{C}^{N\times 1}$ and $\mathbf{w}_k \in \mathbb{C}^{N\times 1}$ are the BF vectors for common and private stream, respectively. The BS sends the composite signal to each device, which is multiplied by the corresponding transmit BF vector before being sent to the device, and then the device employs the SIC scheme for decoding. Based on this, the received signal at U_k can be written as

$$\begin{aligned} y_k = \mathbf{h}_k^H &\left(\sqrt{a_c P_s}\mathbf{w}_c s_c + \textstyle\sum_{k=1}^{K} \sqrt{a_k P_s}\mathbf{w}_k s_k + \boldsymbol{\kappa}_s\right) \\ &+ \kappa_k + n_k, \end{aligned} \tag{2}$$

where $\boldsymbol{\kappa}_s$ is the HWI vector at the transmitter and its i-th element $\kappa_{s,i} \sim CN(0, P_s\tau_s^2)$, and $\kappa_k \sim CN(0, P_s||\mathbf{h}_k||^2\tau_k^2)$ is the HWI at the receiver, where τ_s and τ_k are the level parameters of HWIs at the transmitter and receiver respectively [20] [21] [10]. $n_k \sim CN(0, \sigma_k^2)$ is the complex gaussian noise at U_k and σ_k^2 is the variance of the noise. For the sake of generality, it is assumed that the noise variances are the same at all UDs, i.e. $\sigma_k^2 = \sigma^2$.

The THz channel experiences path loss, molecular absorption effects, misalignment fading and small-scale fading. Correspondingly, the channel vector $\mathbf{h}_k \in \mathbb{C}^{N\times 1}$ can be expressed as [10], [18]

$$\mathbf{h}_k = h_{L,k}\mathbf{g}_k = \frac{c\sqrt{G_s G_k}}{4\pi f d_k}\exp\left(-\kappa_{abs}(f)d_k/2\right)\mathbf{g}_k, \tag{3}$$

where $h_{L,k}$ is path gain, including free-space path loss and molecular absorption loss. $\mathbf{g}_k \in \mathbb{C}^{N\times 1}$ includes misalignment fading and small-scale fading. d_k is the distance between the BS and U_k. G_t and G_r represent the transmit and receive antenna gain, respectively. c is the speed of light, and f is the frequency. $\kappa_{abs}\left(f\right)$ is the molecular absorption coefficient, indicating the energy of electromagnetic waves absorbed by the molecules of the medium, which is related to relative humidity, atmospheric pressure and temperature.

Citation information: DOI 10.1109/JIOT.2025.3565925, IEEE Internet of Things Journal

$$\gamma_c^k = \frac{a_c \gamma_0 h_{L,k}^2 \left|\mathbf{g}_k^H \mathbf{w}_c\right|^2}{a_k \gamma_0 h_{L,k}^2 \left|\mathbf{g}_k^H \mathbf{w}_k\right|^2 + \sum_{j=1, j\neq k}^{j=K} a_j \gamma_0 h_{L,k}^2 \left|\mathbf{g}_k^H \mathbf{w}_j\right|^2 + \gamma_0 h_{L,k}^2 \|\mathbf{g}_k\|^2 (\tau_s^2 + \tau_k^2) + 1}, \tag{4}$$

With (2), the effective signal to interference plus noise ratio (SINR) for U_k decoding s_c can be deduced as (4), which is shown at the top of this page, where the SNR $\gamma_0 = P_s/\sigma^2$. After decoding the common stream s_c, each device uses the SIC scheme to decode the corresponding private stream. Considering the effect of imperfect SIC, the SINR for U_k decoding s_k can be given by

$$\gamma_p^k = \frac{a_k \gamma_0 h_{L,k}^2 \left|\mathbf{g}_k^H \mathbf{w}_k\right|^2}{\sum\limits_{j\neq k}^{K} a_j \gamma_0 h_{L,k}^2 \left|\mathbf{g}_k^H \mathbf{w}_j\right|^2 + \gamma_0 h_{L,k}^2 \|\mathbf{g}_k\|^2 (\tau_s^2+\tau_k^2) + \gamma_0 h_{L,k}^2 \left|\mathbf{g}_k^H \mathbf{w}_c\right|^2 \delta a_c + 1}. \tag{5}$$

where $\delta \in [0, 1]$ is the interference transfer factor [22] [23]. When $\delta = 0$, which corresponds to ideal SIC case, the information will be decoded correctly.

According to [18], we present a BF matrix $\mathbf{W} = \mathbf{G}\left(\mathbf{G}^H\mathbf{G}\right)^{-1}\mathbf{U} = [\mathbf{w}_1, \mathbf{w}_2, ..., \mathbf{w}_K] \in \mathbb{C}^{N\times K}$, where $\mathbf{G} = [\mathbf{g}_1, \mathbf{g}_2, ..., \mathbf{g}_K]$ and $\mathbf{U} = \mathrm{diag}\left(\|\mathbf{g}_1\|, \|\mathbf{g}_2\|, ..., \|\mathbf{g}_K\|\right)$. Each column in the BF matrix $\mathbf{W}$ represents the BF vector $\mathbf{w}_k$ for each device's private stream s_k, and the common stream BF vector $\mathbf{w}_c$ is designed as $\mathbf{w}_c = \sum_{k=1}^K \mathbf{w}_k$. According to the above design, we can obtain $\left|\mathbf{g}_k \mathbf{w}_c\right|^2 = \|\mathbf{g}_k\|^2, \left|\mathbf{g}_k^H \mathbf{w}_k\right|^2 = \|\mathbf{g}_k\|^2, \left|\mathbf{g}_k^H \mathbf{w}_j\right|^2 = 0, 1 \le j \le K$ and $j \neq k$.

Therefore, with the results above, the devices' interference can be removed, and the corresponding equations (4) and (5) can be respectively reduced as

$$\gamma_c^k = \frac{a_c \gamma_0 h_{L,k}^2 \|\mathbf{g}_k\|^2}{\gamma_0 h_{L,k}^2 \|\mathbf{g}_k\|^2 (a_k + \Delta_k) + 1}, \tag{6}$$

and
$$\gamma_p^k = \frac{a_k \gamma_0 h_{L,k}^2 \|\mathbf{g}_k\|^2}{\gamma_0 h_{L,k}^2 \|\mathbf{g}_k\|^2 (\Delta_k + \delta a_c) + 1}, \tag{7}$$

where $\Delta_k = \tau_s^2 + \tau_k^2$. When $\tau_s^2 = \tau_k^2 = 0$, which corresponds to the perfect transceiver hardware, the above two equations are reduced to the (6) in [18]. Besides, when $\delta = 0$, they are reduced to the ones under the perfect SIC. Thus, the above equations include some existing expressions as special cases.

III. Outage probability and PA scheme

In this section, we will analyze the outage performance of the multi-antenna RSMA-THz system in the presence of hardware impairments and imperfect SIC, and derive the PA scheme to minimize the OP. Firstly, we derive the PDF and CDF of the effective channel gains, and then, we derive the OP for the performance analysis and optimization.

For sake of performance analysis, according to [24], the pointing error of each antenna link can be considered to be the same, i.e., the misalignment fading for each antenna link is the same. The gain of the small-scale fading of the channel of the THz link has the statistical characteristics of generalized and easily handled $\alpha-\mu$ fading, which is experimentally validated with excellent fitting accuracy in [25]. On a THz receiver, the sum of N random variables with $\alpha - \mu$ distribution can also be well approximated with a single $\alpha - \mu$ random variable [26]. Thus, we have:

$$\|\mathbf{g}_k\|^2 = h_{p,k}^2 \sum_{n=1}^N |h_{f,k,n}|^2 = h_{p,k}^2 T_k, \tag{8}$$

where $h_{p,k}$ is the misalignment coefficient between the BS and U_k, $T_k = \sum_{n=1}^N |h_{f,k,n}|^2$, $h_{f,k,n}$ is the small-scale fading coefficient between the n-th antenna of BS and U_k, and it is modeled as generalized $\alpha-\mu$ distribution [27]. Thus, the PDF of $|h_{f,k,n}|$ can be written as

$$f_{|h_{f,k,n}|}(x) = \frac{\alpha \mu_k^{\mu_k} x^{\alpha\mu_k - 1}}{\hat{h}_f^{\alpha\mu_k} \Gamma(\mu_k)} \exp\left(-\mu_k \frac{x^\alpha}{\hat{h}_f^\alpha}\right), \tag{9}$$

where α is the fading parameter, μ_k is the normalized variance of fading channel envelope, and $\hat{h}_f$ is α-root mean value of channel envelope. $\Gamma(\cdot)$ is the gamma function. According to [26] [27], T_k can be well approximated with a single $\alpha-\mu$ random variable by using the moment-based estimators. Namely, the new $\hat{\alpha}$ and $\hat{\mu}$ can be attained by solving the following two equations.

$$\begin{cases} \frac{\Gamma^2\left(\hat{\mu}+\frac{2}{\hat{\alpha}}\right)}{\Gamma(\hat{\mu})\Gamma\left(\hat{\mu}+\frac{4}{\hat{\alpha}}\right) - \Gamma^2\left(\hat{\mu}+\frac{2}{\hat{\alpha}}\right)} = \frac{\mathbb{E}^2(T_k)}{\mathbb{E}(T_k^2) - \mathbb{E}^2(T_k)}, \\ \frac{\Gamma^2\left(\hat{\mu}+\frac{4}{\hat{\alpha}}\right)}{\Gamma(\hat{\mu})\Gamma\left(\hat{\mu}+\frac{8}{\hat{\alpha}}\right) - \Gamma^2\left(\hat{\mu}+\frac{4}{\hat{\alpha}}\right)} = \frac{\mathbb{E}^2(T_k^2)}{\mathbb{E}(T_k^4) - \mathbb{E}^2(T_k^2)}, \end{cases} \tag{10}$$

where $\mathbb{E}[T_k^i]$ can be calculated as [26]

$$\mathbb{E}[T_k^i] = \sum_{i_1=0}^{i} \sum_{i_2=0}^{i_1} \cdots \sum_{i_{N-1}=0}^{i_{N-2}} \begin{pmatrix} i \\ i_1 \end{pmatrix} \begin{pmatrix} i_1 \\ i_2 \end{pmatrix} \cdots \begin{pmatrix} i_{N-2} \\ i_{N-1} \end{pmatrix} \times \mathbb{E}\left[\rho_{k,1}^{2(i-i_1)}\right] \mathbb{E}\left[\rho_{k,2}^{2(i_1-i_2)}\right] \cdots \mathbb{E}\left[\rho_{k,N}^{2i_{N-1}}\right], \tag{11}$$

where $\rho_{k,i} = |h_{f,k,i}|, i = 1, ..., N$. The equations (10) above can be solved by means of the Matlab toolbox. With the obtained $\hat{\alpha}$ and $\hat{\mu}$, the parameter $\hat{h}_f$ is updated as [26] [27]

$$\tilde{h}_f = \sqrt{\hat{\mu}^{2/\hat{\alpha}} \Gamma(\hat{\mu}) \mathbb{E}[T_k] / \Gamma(\hat{\mu} + 1/\hat{\alpha})}. \tag{12}$$

Hence, based on the obtained $\hat{\alpha}$, $\hat{\mu}$ and $\tilde{h}_f$, the PDF of T_k can be derived as

$$f_{T_k}(x) = \frac{\hat{\alpha} \hat{\mu}_k^{\hat{\mu}_k} x^{\hat{\alpha}\hat{\mu}_k/2 - 1}}{2\tilde{h}_f^{\hat{\alpha}\hat{\mu}_k} \Gamma(\hat{\mu}_k)} \exp\left(-\hat{\mu}_k \frac{x^{\hat{\alpha}/2}}{\tilde{h}_f^{\hat{\alpha}}}\right), \tag{13}$$

Besides, the PDF of $h_{p,k}^2$ is given by [28]

$$f_{h_{p,k}^2}(x) = \frac{1}{2} \xi_k^2 A_0^{-\xi_k^2} x^{\frac{\xi_k^2}{2} - 1}, 0 \le x \le A_0^2, \tag{14}$$

where A_0 and ξ_k are the parameters of misalignment fading, respectively [28] [15].

This article has been accepted for publication in a future issue of this journal, but has not been fully edited. Content may change prior to final publication.
Citation information: DOI 10.1109/JIOT.2025.3565925, IEEE Internet of Things Journal

Using (13) and (14), the PDF of $\|\mathbf{g}_k\|^2 = h_{p,k}^2 T_k$ can be derived as

$$\begin{aligned} f_{\|\mathbf{g}_k\|^2}(x) &= \textstyle\int_0^{A_0^2} \frac{1}{y} f_{T_k}\left(\frac{x}{y}\right) f_{h_{p,k}^2}(y)dy \\ &= \frac{1}{2}\frac{\xi_k^2}{A_0^{\xi_k^2}}\frac{\hat{\alpha}}{2\Gamma(\hat{\mu}_k)}\left(\frac{\hat{\mu}_k}{\hat{h}_f^{\hat{\alpha}}}\right)^{\hat{\mu}_k} x^{\frac{\hat{\alpha}\hat{\mu}_k}{2}-1} \\ &\times \textstyle\int_0^{A_0^2} \exp\left(-\frac{\hat{\mu}_k}{\hat{h}_f^{\hat{\alpha}}}\left(\frac{x}{y}\right)^{\frac{\hat{\alpha}}{2}}\right) y^{\frac{\xi_k^2}{2}-\frac{\hat{\alpha}\hat{\mu}_k}{2}-1}dy. \end{aligned} \tag{15}$$

Let $z = \frac{\hat{\mu}_k}{\hat{h}_f^{\hat{\alpha}}}\left(\frac{x}{y}\right)^{\frac{\hat{\alpha}}{2}}$, then the PDF of $\|\mathbf{g}_k\|^2$ is given by

$$\begin{aligned} f_{\|\mathbf{g}_k\|^2}(x) &= \frac{1}{2}\frac{\xi_k^2}{A_0^{\xi_k^2}}\frac{1}{\Gamma(\mu_k)}\left(\frac{\hat{\mu}_k}{\hat{h}_f^{\hat{\alpha}}}\right)^{\xi_k^2/\hat{\alpha}} x^{\frac{\xi_k^2}{2}-1} \\ &\times \textstyle\int_{\frac{\hat{\mu}_k}{\hat{h}_f^{\hat{\alpha}}}\left(\frac{x}{A_0^2}\right)^{\frac{\hat{\alpha}}{2}}}^{\infty} \exp(-z)\, z^{-\frac{\xi_k^2}{\hat{\alpha}}+\hat{\mu}_k-1}dz \\ &= \frac{1}{2}\underbrace{\frac{\xi_k^2}{A_0^{\xi^2}}\frac{1}{\Gamma(\hat{\mu}_k)}\frac{\hat{\mu}_k^{\frac{\xi_k^2}{\hat{\alpha}}}}{\tilde{h}_f^{\xi_k^2}}}_{A_k} x^{\frac{\xi_k^2}{2}-1}\Gamma(\underbrace{-\frac{\xi_k^2}{\hat{\alpha}}+\hat{\mu}_k}_{B_k}, \underbrace{\frac{\hat{\mu}_k}{\hat{h}_f^{\hat{\alpha}}}A_0^{-\hat{\alpha}}}_{C_k} x^{\frac{\hat{\alpha}}{2}}) \\ &= \frac{1}{2}A_k x^{\frac{\xi_k^2}{2}-1}\Gamma\left(B_k, C_k x^{\frac{\alpha}{2}}\right), \end{aligned} \tag{16}$$

where $A_k = \frac{\xi_k^2}{(A_0\tilde{h}_f)^{\xi_k^2}}\frac{1}{\Gamma(\hat{\mu}_k)}\hat{\mu}_k^{\frac{\xi_k^2}{\hat{\alpha}}}$, $B_k = \hat{\mu}_k - \frac{\xi_k^2}{\hat{\alpha}}$, $C_k = \frac{\hat{\mu}_k}{\hat{h}_f^{\hat{\alpha}}}A_0^{-\hat{\alpha}}$. $\Gamma(s,x) = \int_x^{\infty} e^{-t}t^{s-1}dt$ is the upper incomplete gamma function [29]. With (16), the CDF of $\|\mathbf{g}_k\|^2$ can be written as

$$\begin{aligned} F_{\|\mathbf{g}_k\|^2}(x) &= \textstyle\int_0^x f_{\|\mathbf{g}_k\|^2}(y)dy \\ &= \textstyle\int_0^x \frac{1}{2}A_k y^{\frac{\xi_k^2}{2}-1}\Gamma(B_k, C_k y^{\frac{\hat{\alpha}}{2}})dy. \end{aligned} \tag{17}$$

Let $\nu = C_k y^{\frac{\hat{\alpha}}{2}}$, and according to $\int x^{a-1}\Gamma(s,x)dx = \left(x^a\Gamma(s,x) - \Gamma(s+a,x)\right)/a$ [30], then the CDF of $\|\mathbf{g}_k\|^2$ is derived as

$$\begin{aligned} F_{\|\mathbf{g}_k\|^2}(x) &= \frac{1}{\hat{\alpha}}A_k C_k^{-\frac{\xi_k^2}{\hat{\alpha}}} \textstyle\int_0^{C_k x^{\frac{\hat{\alpha}}{2}}} \nu^{\frac{\xi_k^2}{\hat{\alpha}}-1}\Gamma(B_k,\nu)d\nu \\ &= \frac{A_k}{\xi_k^2}x^{\frac{\xi_k^2}{2}}\Gamma(B_k, C_k x^{\frac{\hat{\alpha}}{2}}) + \frac{\Upsilon(\hat{\mu}_k, C_k x^{\frac{\hat{\alpha}}{2}})}{\Gamma(\hat{\mu}_k)}, \end{aligned} \tag{18}$$

where $\Upsilon(s,x) = \int_0^x e^{-t}t^{s-1}dt$ is the lower incomplete gamma function [29].

Besides, when $\alpha = 2$, the small-scale $\alpha - \mu$ fading is transformed into the Nakagami-*m* fading [27]. Thus, when the small-scale channel $h_{f,k,n}$ follows Nakagami-*m* fading, the corresponding CDF and PDF of $\|\mathbf{g}_k\|^2$ can be respectively reduced as

$$F_{\|\mathbf{g}_k\|^2}(x) = \frac{\tilde{A}_k}{\xi_k^2}x^{\frac{\xi_k^2}{2}}\Gamma(\tilde{B}_k, \tilde{C}_k x) + \frac{\Upsilon(Nm_k, \tilde{C}_k x)}{\Gamma(Nm_k)}, \tag{19}$$

$$\text{and } f_{\|\mathbf{g}_k\|^2}(x) = \frac{1}{2}\tilde{A}_k x^{\frac{\xi_k^2}{2}-1}\Gamma\left(\tilde{B}_k, \tilde{C}_k x\right), \tag{20}$$

where m_k is the fading parameter of Nakagami-*m* fading, $\tilde{A}_k = \frac{\xi_k^2}{A_0^{\xi_k^2}}\frac{1}{\Gamma(Nm_k)}\frac{m_k^{\xi_k^2/2}}{\hat{h}_f^{\xi_k^2}}$, $\tilde{B}_k = Nm_k - \frac{\xi_k^2}{2}$, $\tilde{C}_k = \frac{m_k}{\hat{h}_f^2}A_0^{-2}$.

A. Outage Probability

Since the BS uses the RSMA scheme to transmit the composite signal of all device's common part and private part, each device decodes the common stream s_c firstly, and then use the SIC scheme to decode the private stream s_k. When the device's target rate is determined by the device's quality of service, the OP is an important criterion for the system evaluation. The device's outage event can be described as: 1) U_k cannot decode s_c correctly; 2) U_k can decode s_c correctly, but cannot decode s_k correctly. For simplifying the calculation of OP, the outage event can be represented by its complement events. Namely, if and only if both the common stream and the corresponding private stream are successfully decoded by U_k, the communication event between BS and U_k can happen. In other words, if only one of γ_c^k and γ_p^k is below their respective thresholds, the link between BS and U_k will interrupt, and correspondingly, the outage event happens. Thus, the OP of U_k is defined as

$$OP_{U_k} = 1 - \Pr\left(\gamma_c^k \geq \gamma_c^{th}, \gamma_p^k \geq \gamma_k^{th}\right) \tag{21}$$

where $\gamma_c^{th} = 2^{R_c^{th}} - 1$, $\gamma_k^{th} = 2^{R_k^{th}} - 1$, R_c^{th} and R_k^{th} are the target rate of the common stream and the private stream separately.

According to (21), using (6) and (7), the OP of U_k can be derived as

$$OP_{U_k} = \begin{cases} F_{\|\mathbf{g}_k\|^2}(\vartheta_k), & \gamma_c^{th} < \frac{a_c}{a_k+\Delta_k} \text{ and } \gamma_k^{th} < \frac{a_k}{\Delta_k+\delta a_c} \\ 1, & else \end{cases} \tag{22}$$

where $\vartheta_k = \max\left(\hat{\gamma}_{c,k}^{th}, \hat{\gamma}_k^{th}\right)$, $\hat{\gamma}_{c,k}^{th} = \frac{\gamma_c^{th}}{(a_c - \gamma_c^{th}(a_k+\Delta_k))\gamma_0 h_{L,k}^2}$, $\hat{\gamma}_k^{th} = \frac{\gamma_k^{th}}{\left(a_k - \gamma_k^{th}(\Delta_k+\delta a_c)\right)\gamma_0 h_{L,k}^2}$.

Substituting equation (19) into (22), the closed-form expression of OP_{U_k} in RSMA-THz communication system can be given by (23), which is shown at the top of next page,

If any one device's communication happens to interrupt, the system will interrupt. Thus, the OP of the system can be expressed as (24), which is shown at the top of next page.

Similarly, the OP of the system over Nakagami fading channels can be deduced as for $\gamma_c^{th} < \frac{a_c}{a_k+\Delta_k}$ and $\gamma_k^{th} < \frac{a_k}{\Delta_k+\delta a_c}$, $OP_{sys} = 1 - \prod_{k=1}^{K}\left(\frac{\Gamma\left(Nm_k, \tilde{C}_k\vartheta_k\right)}{\Gamma(Nm_k)} - \frac{\tilde{A}_k}{\xi_k^2}\vartheta_k^{\frac{\xi_k^2}{2}}\Gamma(\tilde{B}_k, \tilde{C}_k\vartheta_k)\right)$, and else, $OP_{sys} = 1$.

B. Diversity gain

In this subsection, we give an asymptotic analysis of OP at high SNR, and then derive the diversity gain. With (23), we can obtain

$$\begin{aligned} OP_{U_k} &= \frac{A_k}{\xi_k^2}\vartheta_k^{\frac{\xi_k^2}{2}}\Gamma(B_k, C_k\vartheta_k^{\frac{\hat{\alpha}}{2}}) + \frac{\Upsilon(\hat{\mu}_k, C_k\vartheta_k^{\frac{\hat{\alpha}}{2}})}{\Gamma(\hat{\mu}_k)} \\ &= \frac{A_k}{\xi_k^2}(\varphi_k\gamma_0^{-1})^{\frac{\xi_k^2}{2}}\Gamma(B_k, C_k(\varphi_k\gamma_0^{-1})^{\frac{\hat{\alpha}}{2}}) \\ &\quad + \frac{\Upsilon(\hat{\mu}_k, C_k(\varphi_k\gamma_0^{-1})^{\frac{\hat{\alpha}}{2}})}{\Gamma(\hat{\mu}_k)}, \end{aligned} \tag{25}$$

where $\varphi_k = \max\left(\frac{\gamma_c^{th}h_{L,k}^{-2}}{a_c - \gamma_c^{th}(a_k+\Delta_k)}, \frac{\gamma_k^{th}h_{L,k}^{-2}}{a_k - \gamma_k^{th}(\Delta_k+\delta a_c)}\right)$.

Using Eq.(8.354.1) in [29] for $\Upsilon(s,x)$, we have: $\Upsilon(s,x) \approx x^s/s$ for very small x. Correspondingly, $\Gamma(s,x) = \Gamma(s) -$

This article has been accepted for publication in a future issue of this journal, but has not been fully edited. Content may change prior to final publication.
Citation information: DOI 10.1109/JIOT.2025.3565925, IEEE Internet of Things Journal

$$OP_{U_k} = \begin{cases} \frac{A_k}{\xi_k^2}\vartheta_k^{\frac{\xi_k^2}{2}}\Gamma(B_k, C_k\vartheta_k^{\frac{\hat{\alpha}}{2}}) + \frac{\Upsilon(\hat{\mu}_k, C_k\vartheta_k^{\frac{\hat{\alpha}}{2}})}{\Gamma(\hat{\mu}_k)}, & \gamma_c^{th} < \frac{a_c}{a_k+\Delta_k} \text{ and } \gamma_k^{th} < \frac{a_k}{\Delta_k+\delta a_c} \\ 1, & else \end{cases} \tag{23}$$

$$\begin{aligned} OP_{sys} &= 1-(1-OP_{U_1})(1-OP_{U_2})\ldots(1-OP_{U_K}) \\ &= \begin{cases} 1-\prod\limits_{k=1}^{K}\left(\frac{\Gamma\left(\hat{\mu}_k, C_k\vartheta_k^{\frac{\hat{\alpha}}{2}}\right)}{\Gamma(\hat{\mu}_k)} - \frac{A_k}{\xi_k^2}\vartheta_k^{\frac{\xi_k^2}{2}}\Gamma\left(B_k, C_k\vartheta_k^{\frac{\hat{\alpha}}{2}}\right)\right), & \gamma_c^{th} < \frac{a_c}{a_k+\Delta_k} \text{ and } \gamma_k^{th} < \frac{a_k}{\Delta_k+\delta a_c} \\ 1, & else \end{cases} \end{aligned} \tag{24}$$

$\Upsilon(s,x) \approx \Gamma(s) - x^s/s$. Substituting the above approximations for $\Upsilon(s,x)$ and $\Gamma(s,x)$ into (25) yields the asymptotic OP of device k as

$$OP_{U_k}^{asy,\infty} = \frac{A_k\Gamma(B_k)}{\xi_k^2}\varphi_k^{\frac{\xi_k^2}{2}}\gamma_0^{-\frac{\xi_k^2}{2}} - \frac{\xi_k^2 C_k^{\hat{\mu}_k}\varphi_k^{\frac{\hat{\alpha}\hat{\mu}_k}{2}}}{\hat{\alpha}\Gamma(\hat{\mu}_k+1)B_k}\gamma_0^{\frac{-\hat{\alpha}\hat{\mu}_k}{2}}. \tag{26}$$

With (26), we can derive the diversity gain for device k as

$$G_{c,k} = -\lim_{\gamma_0\to\infty}\frac{\log(OP_{U_k}^{asy,\infty})}{\log(\gamma_0)} = \min\{\tfrac{\xi_k^2}{2}, \tfrac{\hat{\alpha}\hat{\mu}_k}{2}\}. \tag{27}$$

Substituting (26) into (24) gives

$$\begin{aligned} &OP_{sys}^{asy,\infty} \\ &= 1-\prod_{k=1}^{K}\left(1+\frac{\xi_k^2 C_k^{\hat{\mu}_k}(\varphi_k\gamma_0^{-1})^{\frac{\hat{\alpha}\hat{\mu}_k}{2}}}{\hat{\alpha}\Gamma(\hat{\mu}_k+1)B_k} - \frac{A_k\Gamma(B_k)(\varphi_k\gamma_0^{-1})^{\frac{\xi_k^2}{2}}}{\xi_k^2}\right). \end{aligned} \tag{28}$$

This is an asymptotic OP of the system at high SNR region. With (28) and (27), by means of the theoretical derivation, the diversity gain of the system can be given by $\min\limits_{1\le k\le K}\{G_{c,k}\}$.

Similarly, we can derive the asymptotic OP of the system at high SNR region for Namkagmi fading channels (i.e, $\alpha = 2$) as follows:

$$\begin{aligned} &OP_{sys}^{asy,\infty} \\ &= 1-\prod_{k=1}^{K}\left(1+\frac{\xi_k^2\tilde{C}_k^{N\mu_k}(\varphi_k\gamma_0^{-1})^{Nm_k}}{2\Gamma(Nm_k+1)\tilde{B}_k} - \frac{\tilde{A}_k\Gamma(\tilde{B}_k)(\varphi_k\gamma_0^{-1})^{\frac{\xi_k^2}{2}}}{\xi_k^2}\right). \end{aligned} \tag{29}$$

C. PA scheme

In this subsection, by minimizing the obtained OP above, we propose an adaptive PA scheme to adjust the PA coefficients between the common stream and private streams for the outage performance improvement.

With (24), subject to the sum power constraint, the OP minimization problem can be formulated as

$$\begin{aligned} &\min_{\{a_c,a_k\}} J = OP_{sys} = 1-\textstyle\prod_{k=1}^{K}(1-OP_{U_k}) \\ &s.t.\ \ a_c + \textstyle\sum_{k=1}^{K} a_k = 1. \end{aligned} \tag{30}$$

From (30), it is found that minimizing the OP_{sys} can be realized by minimizing the OP of each private stream. Namely, by minimizing OP_{U_k} for $k = 1,...,K$, the optimal PA can be attained. With (16), the PDF $f_{\|\mathbf{g}_k\|^2}(x) > 0$. Thus, the CDF $F_{\|\mathbf{g}_k\|^2}(x)$ is a increasing function on $x > 0$. Based on this fact, in terms of (22), minimizing OP_{U_k} is equivalent to minimizing ϑ_k. Hence, in what follows, we will calculate the minimum value of ϑ_k by solving the PA coefficients $\{a_c, a_k\}$.

Considering that $\vartheta_k = \max\left(\hat{\gamma}_{c,k}^{th}, \hat{\gamma}_k^{th}\right)$, we need to discuss two cases for finding the minmum ϑ_k.

1) When $\hat{\gamma}_{c,k}^{th} \ge \hat{\gamma}_k^{th}$, the $\vartheta_k = \hat{\gamma}_{c,k}^{th}$. Correspondingly, minimizing ϑ_k is equivalent to minimizing $\hat{\gamma}_{c,k}^{th}$. From $\hat{\gamma}_{c,k}^{th} = \frac{\gamma_c^{th}}{(a_c-\gamma_c^{th}(a_k+\Delta_k))\gamma_0 h_{L,k}^2}$, it is found that the smaller a_k is, the smaller $\hat{\gamma}_{c,k}^{th}$ is. Since $\hat{\gamma}_{c,k}^{th} \ge \hat{\gamma}_k^{th}$, we can obtain that $a_k \ge \frac{a_c\gamma_k^{th}}{\gamma_c^{th}+\gamma_k^{th}\gamma_c^{th}}$. Hence, we can obtain the optimal a_k as $\frac{a_c\gamma_k^{th}}{\gamma_c^{th}+\gamma_k^{th}\gamma_c^{th}}$ under this case since this value of a_k is the smallest.

2) When $\hat{\gamma}_{c,k}^{th} \le \hat{\gamma}_k^{th}$, the $\vartheta_k = \hat{\gamma}_k^{th}$. Correspondingly, minimizing ϑ_k is equivalent to minimizing $\hat{\gamma}_k^{th}$. From $\hat{\gamma}_k^{th} = \frac{\gamma_k^{th}}{\left(a_k-\gamma_k^{th}(\Delta_k+\delta a_c)\right)\gamma_0 h_{L,k}^2}$, it is found that the larger a_k is, the smaller $\hat{\gamma}_k^{th}$ is. Since $\hat{\gamma}_{c,k}^{th} \le \hat{\gamma}_k^{th}$, we can obtain that $a_k \le \frac{a_c\gamma_k^{th}}{\gamma_c^{th}+\gamma_k^{th}\gamma_c^{th}}$. Hence, the optimal a_k is attained as $\frac{a_c\gamma_k^{th}}{\gamma_c^{th}+\gamma_k^{th}\gamma_c^{th}}$ under this case since this value of a_k is the largest.

According to the analysis above, the optimal a_k can be attained as

$$a_k^* = \frac{a_c\gamma_k^{th}(1+\delta\gamma_c^{th})}{\gamma_c^{th}+\gamma_k^{th}\gamma_c^{th}}. \tag{31}$$

Substituting (31) into the sum power constraint (30), the optimal a_c is given by

$$a_c^* = \frac{\gamma_c^{th}}{\gamma_c^{th}+(1+\delta\gamma_c^{th})\sum_{k=1}^{K}\gamma_k^{th}/(1+\gamma_k^{th})}. \tag{32}$$

Substituting (32) into (31) yields

$$a_k^* = \frac{\gamma_k^{th}(1+\delta\gamma_c^{th})}{(1+\gamma_k^{th})[\gamma_c^{th}+(1+\delta\gamma_c^{th})\sum_{k=1}^{K}\gamma_k^{th}/(1+\gamma_k^{th})]}. \tag{33}$$

With (32) and (33), the adaptive PA scheme can be obtained. Using this PA scheme, the system can achieve lower OP than that with conventional fixed PA scheme. Besides, considering the constrain conditions $\gamma_c^{th} < \frac{a_c}{a_k+\Delta_k}$ and $\gamma_k^{th} < \frac{a_k}{\Delta_k+\delta a_c}$ in (23), we can derive the following condition for the PA scheme, that is, $(1+\gamma_k^{th})[\gamma_c^{th}+(1+\delta\gamma_c^{th})\sum_{k=1}^{K}\gamma_k^{th}/(1+\gamma_k^{th})](\Delta_k + \delta a_c) < 1+\delta\gamma_c^{th}$. In other words, when this condition is met, the PA scheme is valid for decreasing the OP. However, when this condition is not satisfied, the outage probability will become one.

IV. Ergodic rate analysis

In this section, we will give the ergodic rate analysis of the RSMA-THz system with hardware impairment and imperfect SIC, and derive the ESR of the system for the performance

Citation information: DOI 10.1109/JIOT.2025.3565925, IEEE Internet of Things Journal

analysis. To gain further insights, we derive asymptotic values of ESR under high SNR region and the upper bound of ESR. The ergodic rate can provide an effective evaluation of the transmission data rate over a fading channel.

A. Ergodic sum rate

The achievable rate for U_k decoding the common stream s_c can be expressed as

$$R_c^k = \log_2\left(1+\gamma_c^k\right), \tag{34}$$

where γ_c^k is given as (6). Correspondingly, the ergodic rate for U_k decoding the common stream s_c is written as

$$\bar{R}_c^k = \mathbb{E}\left[R_c^k\right]. \tag{35}$$

According to the principle of RSMA scheme, in order to ensure that all devices can successfully decode the common stream, the ergodic rate of the common stream needs to satisfy that $\bar{R}_c = \min\limits_{1\le k\le K} \bar{R}_c^k$ in terms of [31]–[34].

The achievable rate for U_k decoding the private stream s_k can be expressed as

$$R_p^k = \log_2\left(1+\gamma_p^k\right), \tag{36}$$

where γ_p^k is given as (7). Correspondingly, the ergodic rate for U_k decoding the private stream s_k is written as

$$\bar{R}_p^k = \mathbb{E}\left[R_p^k\right]. \tag{37}$$

Therefore, the ESR of RSMA-THz system is given by [31]

$$\bar{R}_{all} = \min_{k\in K}\bar{R}_c^k + \sum\nolimits_{i=1}^{K}\bar{R}_p^k, \tag{38}$$

With (16), (34) and (35), the theoretical expression of $\bar{R}_c^k$ in (35) can be derived as

$$\begin{aligned}\bar{R}_c^k &= \int_0^\infty \log_2\left(1+\tfrac{a_c h_{L,k}^2\gamma_0 x}{h_{L,k}^2\gamma_0 x(a_k+\Delta_k)+1}\right) f_{\|\mathbf{g}_k\|^2}(x)dx \\ &= \tfrac{1}{2}A_k\int_0^\infty \log_2\left(1+\tfrac{a_c h_{L,k}^2\gamma_0 x}{h_{L,k}^2\gamma_0 x(a_k+\Delta_k)+1}\right) \\ &\qquad \times x^{\frac{\xi_k^2}{2}-1}\Gamma\left(B_k, C_k x^{\frac{\hat{\alpha}}{2}}\right)dx.\end{aligned} \tag{39}$$

Because $\log_2\left(1+\frac{A}{B}\right) = \log_2(B+A)-\log_2(B)$ and $\log_2(x)=\frac{\ln x}{\ln 2}$, $\bar{R}_c^k$ can be further expressed as

$$\begin{aligned}\bar{R}_c^k = &\tfrac{1}{2\ln 2}A_k\int_0^\infty \ln\left(1+h_{L,k}^2\gamma_0 x\left(a_c+a_k+\Delta_k\right)\right) \\ &\qquad \times x^{\frac{\xi_k^2}{2}-1}\Gamma\left(B_k, C_k x^{\frac{\hat{\alpha}}{2}}\right)dx \\ &-\tfrac{1}{2\ln 2}A_k\int_0^\infty \ln\left(1+h_{L,k}^2\gamma_0 x\left(a_k+\Delta_k\right)\right) \\ &\qquad \times x^{\frac{\xi_k^2}{2}-1}\Gamma\left(B_k, C_k x^{\frac{\hat{\alpha}}{2}}\right)dx.\end{aligned} \tag{40}$$

Utilizing the equalities $\ln(1+x) = G_{2,2}^{1,2}\left[x\,\middle|\,\begin{matrix}1,1\\1,0\end{matrix}\right]$ and $\Gamma(b,cx) = G_{1,2}^{2,0}\left[cx\,\middle|\,\begin{matrix}1\\0,b\end{matrix}\right]$ [34] [35], the above equation can be deduced as (41), which is shown at the top of next page, where $G_{p,q}^{m,n}\left(\begin{matrix}\{a_j\}_{j=1:p}\\\{b_j\}_{j=1:q}\end{matrix}\,\middle|\,z\right) = \frac{1}{2\pi i}\oint_L \frac{\left\{\prod_{j=1}^m\Gamma(b_j+s)\right\}\left\{\prod_{j=1}^n\Gamma(1-a_j-s)\right\}}{\left\{\prod_{j=m+1}^q\Gamma(1-b_j-s)\right\}\left\{\prod_{j=n+1}^p\Gamma(b_j+s)\right\}}z^{-s}ds$ is the Meijer-G function [29].

According to the results in [36], we have the following equation (42), which is shown at the top of next page, where $H_{c,d}^{a,b}\left[\cdot\middle|\cdot\right]$ is the Fox-H function, and defined as [37]

$$\begin{aligned}&H_{p,q}^{m,n}\left(\begin{matrix}\{(a_j,\alpha_j)\}_{j=1:p}\\\{(b_j,\beta_j)\}_{j=1:q}\end{matrix}\,\middle|\,z\right)\\ &= \tfrac{1}{2\pi i}\oint_L \tfrac{\left\{\prod_{j=1}^m\Gamma(b_j+\beta_j s)\right\}\left\{\prod_{j=1}^n\Gamma(1-a_j-\hat{\alpha}_j s)\right\}}{\left\{\prod_{j=m+1}^q\Gamma(1-b_j-\beta_j s)\right\}\left\{\prod_{j=n+1}^p\Gamma(a_j+\alpha_j s)\right\}}z^{-s}ds.\end{aligned} \tag{43}$$

Hence, the ergodic rate $\bar{R}_c^k$ for U_k decoding s_c in RSMA-THz system can be given by

$$\begin{aligned}\bar{R}_c^k = \frac{1}{2\ln 2}A_k[&\Phi_{1,k}(h_{L,k}^2\gamma_0(a_c+a_k+\Delta_k)) \\ &-\Phi_{1,k}(h_{L,k}^2\gamma_0(a_k+\Delta_k))],\end{aligned} \tag{44}$$

where $\Phi_{1,k}(x)$ is expressed as

$$\begin{aligned}&\Phi_{1,k}(x)\\ &= x^{-\frac{\xi_k^2}{2}}H_{3,4}^{4,1}\left(\frac{C_k}{x^{\frac{\hat{\alpha}}{2}}}\,\middle|\,\begin{matrix}(-\frac{\xi_k^2}{2},\frac{\hat{\alpha}}{2}),(1-\frac{\xi_k^2}{2},\frac{\hat{\alpha}}{2}),(1,1)\\(0,1),(B_k,1),(-\frac{\xi_k^2}{2},\frac{\hat{\alpha}}{2}),(-\frac{\xi_k^2}{2},\frac{\hat{\alpha}}{2})\end{matrix}\right).\end{aligned} \tag{45}$$

Similarly, the closed-form expression of the ergodic rate $\bar{R}_p^k$ in (37) for U_k decoding the private stream s_k can be derived as

$$\begin{aligned}\bar{R}_p^k = \frac{1}{2\ln 2}A_k[&\Phi_{1,k}\left(h_{L,k}^2\gamma_0(a_k+\Delta_k+\delta a_c)\right) \\ &-\Phi_{1,k}\left(h_{L,k}^2\gamma_0(\Delta_k+\delta a_c)\right)].\end{aligned} \tag{46}$$

Substituting (44) and (46) into (38), the closed-form expression of the ESR $\bar{R}_{all}$ is given by

$$\begin{aligned}\bar{R}_{all} = &\min_{1\le k\le K}[\frac{1}{2\ln 2}A_k(\Phi_{1,k}(h_{L,k}^2\gamma_0(a_c+a_k+\tau_s^2)) \\ &\qquad -\Phi_{1,k}(h_{L,k}^2\gamma_0(a_k+\Delta_k)))] \\ &+\sum_{k=1}^{K}\frac{1}{2\ln 2}A_k[\Phi_{1,k}(h_{L,k}^2\gamma_0(a_k+\Delta_k+\delta a_c)) \\ &\qquad -\Phi_{1,k}(h_{L,k}^2\gamma_0(\Delta_k+\delta a_c))].\end{aligned} \tag{47}$$

It is found that when the SNR $\gamma_0 = P_s/\sigma^2$ approaches infinity, the ESR $\bar{R}_{all}$ will tend to a fixed value. This is because when $\gamma_0\to\infty$, Eq. (6) and (7) will be simplified as

$$\lim_{\gamma_0\to\infty}\gamma_c^k = \frac{a_c}{(a_k+\Delta_k)} \text{ and } \lim_{\gamma_0\to\infty}\gamma_p^k = \frac{a_k}{\Delta_k+\delta a_c}. \tag{48}$$

Thus, the asymptotic expression of the ESR at high SNR region $\bar{R}_{all}^{asy,\infty}$ is attained as

$$\begin{aligned}&\bar{R}_{all}^{asy,\infty} = \lim_{\gamma_0\to\infty}\bar{R}_{all}\\ &= \min_{1\le k\le K}\left(\log_2(1+\tfrac{a_c}{a_k+\Delta_k})\right)+\sum_{k=1}^{K}\log_2\left(1+\tfrac{a_k}{\Delta_k+\delta a_c}\right).\end{aligned} \tag{49}$$

Remark: As shown in (49), when the SNR is very large, the system ESR tends to be fixed, and is no longer related to the SNR. This asymptotic ESR only depends on the hardware impairments parameter as well as interference transfer factor and the power allocation coefficient of RSMA.

This article has been accepted for publication in a future issue of this journal, but has not been fully edited. Content may change prior to final publication.
Citation information: DOI 10.1109/JIOT.2025.3565925, IEEE Internet of Things Journal

$$\begin{aligned}\bar{R}_c^k = & \tfrac{1}{2\ln 2} A_k \int_0^\infty x^{\frac{\xi_k^2}{2}-1} G_{2,2}^{1,2}\left[h_{L,k}^2 \gamma_0 \left(a_c + a_k + \Delta_k\right) x \,\middle|\, \begin{matrix} 1,1 \\ 1,0 \end{matrix}\right] G_{1,2}^{2,0}\left[C_k x^{\frac{\hat{\alpha}}{2}}, \,\middle|\, \begin{matrix} 1 \\ 0, B_k \end{matrix}\right] dx \\ & - \tfrac{1}{2\ln 2} A_k \int_0^\infty x^{\frac{\xi_k^2}{2}-1} G_{2,2}^{1,2}\left[h_{L,k}^2 \gamma_0 \left(a_k + \Delta_k\right) x \,\middle|\, \begin{matrix} 1,1 \\ 1,0 \end{matrix}\right] G_{1,2}^{2,0}\left[C_k x^{\frac{\hat{\alpha}}{2}}, \,\middle|\, \begin{matrix} 1 \\ 0, B_k \end{matrix}\right] dx,\end{aligned} \tag{41}$$

$$\begin{aligned}&\int_0^\infty \tau^{\alpha-1} G_{u,v}^{s,t}\left(\sigma\tau \,\middle|\, \begin{matrix} c_1, c_2, \cdots, c_u \\ d_1, d_2, \cdots, d_v \end{matrix}\right) G_{p,q}^{m,n}\left(\omega\tau^r \,\middle|\, \begin{matrix} a_1, a_2, \cdots, a_p \\ b_1, b_2, \cdots, b_q \end{matrix}\right) d\tau \\ &= \sigma^{-\alpha} H_{p+v,q+u}^{m+t,n+s}\left(\tfrac{\omega}{\sigma^r} \,\middle|\, \begin{matrix} (a_1,1), \cdots, (a_n,1), (1-\alpha-d_1, r), \cdots, (1-\alpha-d_v, r), (a_{n+1},1), \cdots, (a_p,1) \\ (b_1,1), \cdots, (b_m,1), (1-\alpha-c_1, r), \cdots, (1-\alpha-c_u, r), (b_{m+1},1), \cdots, (b_q,1) \end{matrix}\right),\end{aligned} \tag{42}$$

B. Upper bound of ergodic sum rate

In order to simplify the calculation of ESR, we will give the derivation of a simple upper bound of ESR in this subsection, where the following Lemma 1 is utilized.

Lemma 1. *For the positive numbers A and B, it can be shown that the function $f(x) = \log_2(1 + Ax/(1+Bx))$, $x \geq 0$, is a concave function.*

Proof: Please refer to Appendix A. ■

According to the Jensen's inequality [38], for a concave function $f(x)$, we have: $\mathbb{E}(f(x)) \leq f(\mathbb{E}(x))$. Based on this, we can get

$$\mathbb{E}\left(\log_2\left(1 + \frac{Ax}{Bx+1}\right)\right) \leq \log_2\left(1 + \frac{A\mathbb{E}(x)}{B\mathbb{E}(x)+1}\right). \tag{50}$$

Therefore, with (35) and (37), we have:

$$\bar{R}_c^k \leq \log_2\left(1 + \frac{a_c h_{L,k}^2 \gamma_0 \mathbb{E}\left(\|\mathbf{g}_k\|^2\right)}{1 + h_{L,k}^2 \gamma_0 \mathbb{E}\left(\|\mathbf{g}_k\|^2\right)(a_k + \Delta_k)}\right), \tag{51}$$

$$\bar{R}_p^k \leq \log_2\left(1 + \frac{a_k \gamma_0 h_{L,k}^2 \mathbb{E}\left(\|\mathbf{g}_k\|^2\right)}{1 + \gamma_0 h_{L,k}^2 \mathbb{E}\left(\|\mathbf{g}_k\|^2\right)(\Delta_k + \delta a_c)}\right). \tag{52}$$

To facilitate derivation, the Lemma 2 is also introduced.

Lemma 2. *For the positive numbers $\{b_k\}$ and $\{c_k\}$, $k = 1,...K$, if $b_k \leq c_k$ for $k = 1,...K$, then we have: $\min\limits_{1\leq k\leq K} b_k \leq \min\limits_{1\leq k\leq K} c_k$.*

Proof: Please refer to Appendix B. ■

Considering that $\bar{R}_c = \min\limits_{1\leq k\leq K} \bar{R}_c^k$, using the Lemma 2 and (51), we can obtain the upper bound of $\bar{R}_c^k$ as

$$\begin{aligned}\bar{R}_c &= \min_{1\leq k\leq K} \bar{R}_c^k \\ &\leq \min_{1\leq k\leq K} \log_2\left(1 + \frac{a_c h_{L,k}^2 \gamma_0 \mathbb{E}\left(\|\mathbf{g}_k\|^2\right)}{1 + h_{L,k}^2 \gamma_0 \mathbb{E}\left(\|\mathbf{g}_k\|^2\right)(a_k + \Delta_k)}\right).\end{aligned} \tag{53}$$

According to (38), the upper bound of the ESR of the RSMA-THz system can be given by

$$\begin{aligned}\bar{R}_{all} \leq \bar{R}_{all}^{upper} = &\min_{1\leq k\leq K} \log_2\left(1 + \tfrac{a_c h_{L,k}^2 \gamma_0 \mathbb{E}\left(\|\mathbf{g}_k\|^2\right)}{1 + h_{L,k}^2 \gamma_0 \mathbb{E}\left(\|\mathbf{g}_k\|^2\right)(a_k + \Delta_k)}\right) \\ &+ \sum_{i=1}^K \log_2\left(1 + \tfrac{a_k \gamma_0 h_{L,k}^2 \mathbb{E}\left(\|\mathbf{g}_k\|^2\right)}{1 + \gamma_0 h_{L,k}^2 \mathbb{E}\left(\|\mathbf{g}_k\|^2\right)(\Delta_k + \delta a_c)}\right),\end{aligned} \tag{54}$$

where $\mathbb{E}\left(\|\mathbf{g}_k\|^2\right)$ can be calculated by using (16), i.e.,

$$\begin{aligned}\mathbb{E}\left(\|\mathbf{g}_k\|^2\right) &= \int_0^\infty x f_{\|\mathbf{g}_k\|^2}(x)\, dx \\ &= \tfrac{1}{2} A_k \int_0^\infty x^{\frac{\xi_k^2}{2}} \Gamma(B_k, C_k x^{\frac{\hat{\alpha}}{2}}) dx.\end{aligned} \tag{55}$$

Let $C_k x^{\frac{\hat{\alpha}}{2}} = y$, using $\int_0^\infty x^{a-1} \Gamma(b,x)\, dx = (\Gamma(a+b))/a$, then the above equation can be further expressed as

$$\begin{aligned}\mathbb{E}\left(\|\mathbf{g}_k\|^2\right) &= \tfrac{1}{\hat{\alpha}} \left(\tfrac{1}{C_k}\right)^{\frac{2+\xi_k^2}{\hat{\alpha}}} A_k \int_0^\infty y^{\frac{2+\xi_k^2-\hat{\alpha}}{\hat{\alpha}}} \Gamma(B_k, y) dy \\ &= \left(\tfrac{1}{C_k}\right)^{\frac{2+\xi_k^2}{\hat{\alpha}}} A_k \tfrac{\Gamma\left(\frac{2}{\hat{\alpha}} + \hat{\mu}_k\right)}{2+\xi_k^2} = \tfrac{(\xi_k A_0 \tilde{h}_f)^2}{2+\xi_k^2} \tfrac{\Gamma(2/\hat{\alpha} + \hat{\mu}_k)}{(\hat{\mu}_k)^{2/\hat{\alpha}} \Gamma(\hat{\mu}_k)},\end{aligned} \tag{56}$$

Substituting (56) into (54), the upper bound of the ESR of the system can be attained as (57), which is shown at the top of next page.

C. Special case

In this subsection, we give the ESR analysis under a special case of $\alpha = 2$. When $\alpha = 2$, the small-scale fading obeys the Nakagami-*m* fading, and corresponding $\mu_k = m_k$. Using (20) and (41), the closed-form expression of $\bar{R}_c^k$ for U_k decoding the common stream s_c can be derived as (58), which is shown at the top of next page.

Using the equation in [36], i.e., Eq.(59), which is shown at the middle of next page, we can derive the closed-form expression of $\bar{R}_c^k$ in (58) as

$$\begin{aligned}\bar{R}_c^k = \frac{1}{2\ln 2} \tilde{A}_k &\left[\Phi_{2,k}\left(h_{L,k}^2 \gamma_0 (a_c + a_k + \Delta_k)\right)\right. \\ &\left. - \Phi_{2,k}\left(h_{L,k}^2 \gamma_0 (a_k + \Delta_k)\right)\right],\end{aligned} \tag{60}$$

where $\Phi_{2,k}(x)$ is expressed as

$$\Phi_{2,k}(x) = \tilde{C}_k^{-\frac{\xi_k^2}{2}} G_{4,3}^{1,4}\left(\frac{x}{\tilde{C}_k} \,\middle|\, \begin{matrix} 1, 1, 1 - \frac{\xi_k^2}{2}, 1 - \frac{\xi_k^2}{2} - \tilde{B}_k \\ 1, -\frac{\xi_k^2}{2}, 0 \end{matrix}\right). \tag{61}$$

This article has been accepted for publication in a future issue of this journal, but has not been fully edited. Content may change prior to final publication.
Citation information: DOI 10.1109/JIOT.2025.3565925, IEEE Internet of Things Journal

$$\bar{R}_{all}^{upper}=\min_{1\le k\le K}\log_2\left(1+\frac{\frac{a_c h_{L,k}^2\gamma_0}{C_k^{(2+\xi_k^2)/\hat{\alpha}}}\frac{A_k\Gamma\left(\frac{2}{\hat{\alpha}}+\hat{\mu}_k\right)}{2+\xi_k^2}}{1+\frac{h_{L,k}^2\gamma_0}{C_k^{(2+\xi_k^2)/\hat{\alpha}}}\frac{A_k\Gamma\left(\frac{2}{\hat{\alpha}}+\hat{\mu}_k\right)}{2+\xi_k^2}(a_k+\Delta_k)}\right)+\sum_{i=1}^{K}\log_2\left(1+\frac{a_k\gamma_0 h_{L,k}^2 C_k^{-\frac{2+\xi_k^2}{\hat{\alpha}}}\frac{A_k\Gamma\left(\frac{2}{\hat{\alpha}}+\hat{\mu}_k\right)}{2+\xi_k^2}}{1+\gamma_0 h_{L,k}^2 C_k^{-\frac{2+\xi_k^2}{\hat{\alpha}}}\frac{A_k\Gamma\left(\frac{2}{\hat{\alpha}}+\hat{\mu}_k\right)}{2+\xi_k^2}(\Delta_k+\delta a_c)}\right). \tag{57}$$

$$\begin{aligned}\bar{R}_c^k=&\tfrac{1}{2\ln 2}\tilde{A}_k\int_0^\infty x^{\frac{\xi_k^2}{2}-1}G_{1,2}^{2,0}\left[\tilde{C}_k x,\left|\begin{matrix}1\\0,\tilde{B}_k\end{matrix}\right.\right]G_{2,2}^{1,2}\left[h_{L,k}^2\gamma_0\left(a_c+a_k+\Delta_k\right)x\left|\begin{matrix}1,1\\1,0\end{matrix}\right.\right]dx\\&-\tfrac{1}{2\ln 2}\tilde{A}_k\int_0^\infty x^{\frac{\xi_k^2}{2}-1}G_{1,2}^{2,0}\left[\tilde{C}_k x,\left|\begin{matrix}1\\0,\tilde{B}_k\end{matrix}\right.\right]G_{2,2}^{1,2}\left[h_{L,k}^2\gamma_0\left(a_k+\Delta_k\right)x\left|\begin{matrix}1,1\\1,0\end{matrix}\right.\right]dx.\end{aligned} \tag{58}$$

$$\begin{aligned}&\int_0^\infty \tau^{\alpha-1}G_{u,v}^{s,t}\left(\tau w\left|\begin{matrix}c_1,...,c_t,c_{t+1},...,c_u\\d_1,...,d_s,d_{s+1},...,d_v\end{matrix}\right.\right)G_{p,q}^{m,n}\left(\tau z\left|\begin{matrix}a_1,...,a_n,a_{n+1},...,a_p\\b_1,...,b_m,b_{m+1},...,b_q\end{matrix}\right.\right)d\tau\\&=w^{-\alpha}G_{v+p,u+q}^{m+t,n+s}\left(\tfrac{z}{w}\left|\begin{matrix}a_1,...,a_n,1-\alpha-d_1,...,1-\alpha-d_s,1-\alpha-d_{s+1},...,1-\alpha-d_v,a_{n+1},...,a_p\\b_1,...,b_m,1-\alpha-c_1,...,1-\alpha-c_t,1-\alpha-c_{t+1},...,1-\alpha-c_u,b_{m+1},...,b_q\end{matrix}\right.\right).\end{aligned} \tag{59}$$

Similarly, we can derive the closed-form expression of $\bar{R}_p^k$ for U_k decoding the private stream s_k under small-scale Nakagami-*m* fading, i.e.,

$$\begin{aligned}\bar{R}_p^k=\frac{1}{2\ln 2}\tilde{A}_k&\left[\Phi_{2,k}\left(h_{L,k}^2\gamma_0\left(a_k+\Delta_k+\delta a_c\right)\right)\right.\\&\left.-\Phi_{2,k}\left(h_{L,k}^2\gamma_0(\Delta_k+\delta a_c)\right)\right].\end{aligned} \tag{62}$$

Substituting (60) and (62) into (38), we can obtain the closed-form expression of the ESR $\bar{R}_{all}$ under small-scale Nakagami-*m* fading ($\alpha=2$) as follows.

$$\begin{aligned}\bar{R}_{all}=&\min_{1\le k\le K}\left[\tfrac{1}{2\ln 2}\tilde{A}_k(\Phi_{2,k}(h_{L,k}^2\gamma_0(a_c+a_k+\Delta_k))\right.\\&\left.-\Phi_{2,k}(h_{L,k}^2\gamma_0(a_k+\Delta_k))\right]\\&+\textstyle\sum_{k=1}^{K}\tfrac{1}{2\ln 2}\tilde{A}_k\left[\Phi_{2,k}(h_{L,k}^2\gamma_0(a_k+\Delta_k+\delta a_c))\right.\\&\left.-\Phi_{2,k}(h_{L,k}^2\gamma_0(\Delta_k+\delta a_c))\right]\end{aligned} \tag{63}$$

When $\alpha=2$, with (20), we can obtain the upper bound of the system ESR under small-scale Nakagami-*m* fading, i.e., Eq.(64), which is shown at the middle of next page.

V. Simulation Results

In this section, we present the simulation results to validate the theoretical analysis of outage probability and ergodic sum rate, and evaluate the impacts of different parameters on the system performance. Unless otherwise specified, the main parameters in simulation are listed in Table I. Other parameters are set as: $\kappa_{abs}(f)=0.0033$, $\xi=\xi_k=3.813$ and $A_0=0.39$ [14] [15] [18]. Simulation results are illustrated in Figs. 2-11.

Fig. 2 illustrates the OP of RSMA-THz system with different hardware impairment levels, where $\tau=0,0.1,0.15$. As shown in Fig. 2, the theoretical and simulation values are close to each other, which shows the accuracy of the derived theoretical OP. Also their values have very small deviation, which is due to the fact that we use single $\alpha-\mu$ fading to approximate the multi-antenna $\alpha-\mu$ fading. Besides, the asymptotic OP agrees the simulation well at high SNR, which indicates the accuracy of asymptotic analysis. With the hardware impairment level τ increasing, the outage performance becomes worse due to the larger hardware impairment. Namely, the system with $\tau=0.15$ has higher OP than that with $\tau=0.1$. Moreover, the system with hardware impairment has worse outage performance than that without hardware impairment ($\tau=0$), as expected.

TABLE I
Simulation parameters

Parameters	Default Values
Number of antennas	$N=64$
Number of users	$K=10$
Antenna gain	$G_t=G_r=55$dBi
Frequency	$f=300$GHz
Rate thresholds	R_c^{th} = 1.5bit/s/Hz, R_k^{th} = 0.5bit/s/Hz
PA coefficients	$a_c=0.4$, $a_k=(1-a_c)/K$
Distances	$d_k=20$m
HWI levels	$\tau=\tau_s=\tau_k=0.15$
Fading parameters	$\alpha=4$, $\mu=\mu_k=4$
Interference transfer factor	$\delta=0.2$

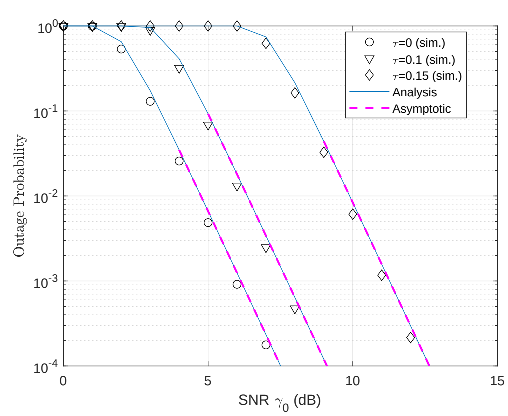

Fig. 2. The OP of the system with different hardware impairment levels.

In Fig, 3, the impact of imperfect SIC on the outage performance of RSMA-THz system is assessed, where different interference transfer factors $\delta=0,0.1,0.2$ are considered.

This article has been accepted for publication in a future issue of this journal, but has not been fully edited. Content may change prior to final publication.
Citation information: DOI 10.1109/JIOT.2025.3565925, IEEE Internet of Things Journal

$$\bar{R}_{all}^{upper} = \min_{1\le k\le K} \log_2\left(1+\frac{a_c h_{L,k}^2\gamma_0 \tilde{C}_k^{-\frac{2+\xi_k^2}{2}} \frac{\tilde{A}_k\Gamma(1+Nm_k)}{2+\xi_k^2}}{1+h_{L,k}^2\gamma_0\tilde{C}_k^{-\frac{2+\xi_k^2}{2}}\frac{\tilde{A}_k\Gamma(1+Nm_k)(a_k+\Delta_k)}{2+\xi_k^2}}\right)+\sum_{i=1}^{K} \log_2\left(1+\frac{a_k\gamma_0 h_{L,k}^2 \tilde{C}_k^{-\frac{2+\xi_k^2}{2}}\frac{\tilde{A}_k\Gamma(1+Nm_k)}{2+\xi_k^2}}{1+\gamma_0 h_{L,k}^2\tilde{C}_k^{-\frac{2+\xi_k^2}{2}}\frac{\tilde{A}_k\Gamma(1+Nm_k)(\Delta_k+\delta a_c)}{2+\xi_k^2}}\right). \tag{64}$$

From Fig. 3, we can observe that the outage performance is greatly affected by the decoding error from the SIC. This is because imperfect SIC decoding brings the device's interference increase, and resultant outage performance will become worse. Namely, the system with perfect SIC $\delta = 0$ has better outage performance than that with imperfect SIC $\delta > 0$, and the system with $\delta = 0.1$ has lower OP than that with $\delta = 0.2$. Besides, the theoretical OP is close to the corresponding simulation, and the asymptotic OP can also match the simulation well at high SNR, which further shows the validity of the presented theoretical analysis of OP.

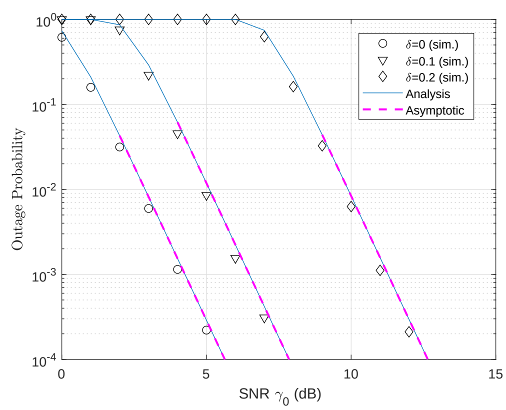

Fig. 3. The OP of the system with different interference transfer factors.

In Fig. 4, we plot the OP of RSMA-THz system with different misalignment fading parameters ξ, where ξ=1.906, 2.859, 3.813. As shown in Fig. 4, the OP of the system becomes smaller with the increase of ξ due to better alignment. Moreover, the system can obtain higher diversity gain as the ξ increases. This is because under this case, the diversity gain is determined by $\xi^2/2$. Thus, the system with ξ=3.813 has higher diversity gain than that with ξ=2.859, and corresponding lower OP is attained. Similarly, the system with ξ=2.859 has lower OP and higher diversity gain than that with ξ=1.906. Besides, the theoretical OP and asymptotic OP can also match the corresponding simulation results well.

Fig. 5 illustrates the OP of RSMA-THz system with different antenna numbers, where $N = 16, 32, 64$, and the proposed adaptive PA (APA) scheme is used for comparison. As shown in Fig. 5, with the increase of antenna number N, the outage performance is effectively increased since more antenna is used. Specifically, the system with $N = 64$ has lower OP than that with $N = 32$, and the system with $N = 32$ has lower OP than that with $N = 16$. Besides, the system with APA scheme has better performance than that with the given fixed PA (FPA) scheme. This is because the former employs the optimized PA and can adapt to the change of the system parameters, while

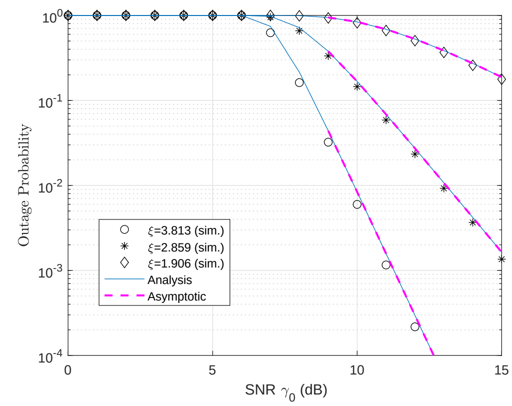

Fig. 4. The OP of the system with different misalignment fading parameters.

the latter uses the fixed PA. The results above indicate that the proposed PA scheme is effective for improving the outage performance.

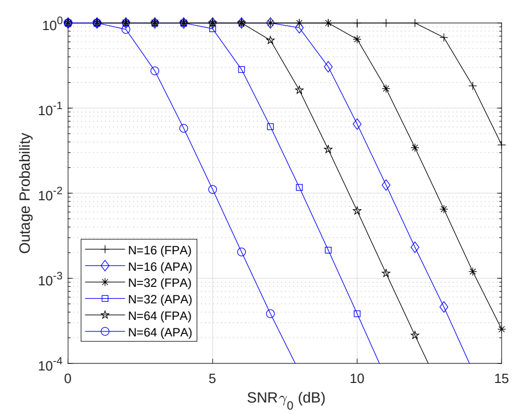

Fig. 5. The OP of the system with different antenna numbers.

Fig. 6 shows the ESR of RSMA-THz system with different hardware impairment levels, where $\tau = 0, 0.1, 0.15$. As observed in Fig. 6, the ESR is effectively increased with the decrease of hardware impairment level due to weaker impairment, i.e., the system with $\tau = 0.1$ can obtain higher ESR than that with $\tau = 0.15$. Moreover, the system with perfect hardware ($\tau = 0$) has higher ESR than that with hardware impairment, as expected. Besides, the simulation results agree well with the corresponding theoretical values, validating the accuracy of the derived theoretical ESR. Additionally, the asymptotic ESR values under high SNR region reveal that the ESR does tend to a constant value at high SNR. Also, this value is dependent on the hardware impairments level, confirming the accuracy of the derived asymptotic ESR.

Citation information: DOI 10.1109/JIOT.2025.3565925, IEEE Internet of Things Journal

Furthermore, the derived upper bound of the ESR has slightly higher value than the corresponding theoretical ESR, which illustrates that the derived upper bound is also valid, and can provide simpler approximate calculation for the ESR due to its simpler expression.

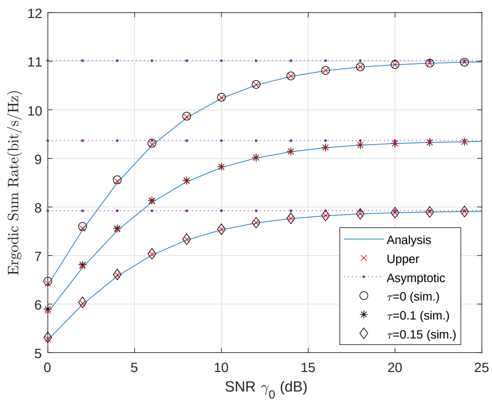

Fig. 6. The ESR of the system with different hardware impairment levels.

In Fig. 7, we plot the ESR of RSMA-THz system with different interference transfer factors, where $\delta = 0, 0.1, 0.2$. From Fig. 7, we can see that the system with perfect SIC ($\delta = 0$) has higher ESR than that with imperfect SIC ($\delta = 0.1, 0.2$), as expected. Moreover, due to larger imperfection of SIC, the system with $\delta = 0.2$ has lower ESR than that with $\delta = 0.1$. Besides, the theoretical ESR has the values very close to the corresponding simulations, and asymptotic ESR at high SNR also tends to the constant value. Furthermore, the upper bound of the ESR is slightly higher than the corresponding theoretical one. These results above further show the effectiveness of the presented theoretical rate analysis.

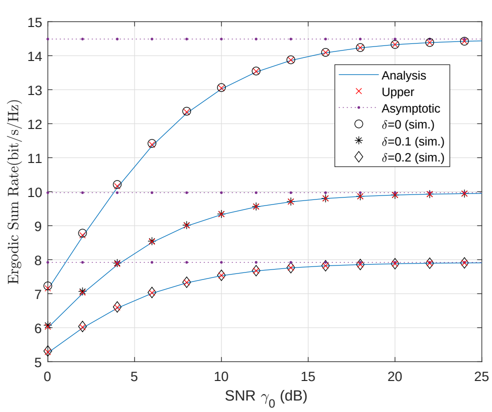

Fig. 7. The ESR of the system with different interference transfer factors.

Fig. 8 illustrates the ESR of RSMA-THz system with different antenna numbers and misalignment fading parameters, where $N = 16, 32, 64$, and $\xi = 1.906, 3.813$. As shown in Fig. 8, the ESR is effectively increased as the antenna number N increases since more antennas are used. Specifically, the system with $N = 64$ has higher ESR than that with $N = 32$, and the system with $N = 32$ has higher ESR than that with $N = 16$. Moreover, with the increases of misalignment fading parameter ξ, the system can also obtain higher ESR due to better alignment. Namely, the system with $\xi = 3.813$ has larger ESR than that with $\xi = 1.906$, as expected. Besides, the theoretical ESR can match the corresponding simulations well, and asymptotic ESR at high SNR also tends to the constant value, which is not related to the N, ξ and SNR.

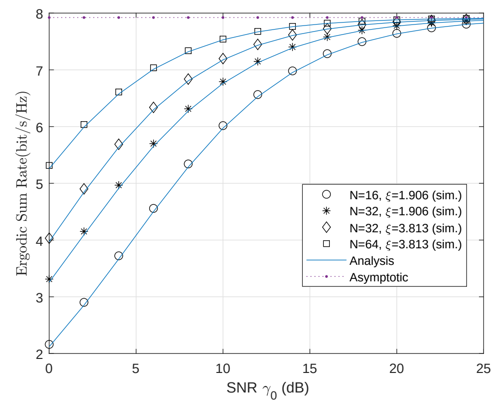

Fig. 8. The ESR of the system with different antenna numbers and misalignment fading parameters.

Fig. 9 gives the ESR of RSMA-THz system with different user numbers, where $K = 5, 10, 15$. From Fig. 9, we can observe that the theoretical values of ESR can match the corresponding simulations well, and they are slightly lower than the corresponding upper bounds. Moreover, the asymptotic ESR values at high SNR also tend to the constant values. The above results indicate that the presented theoretical analysis is also effective for different user numbers. Besides, with the increase of user number K, the ESR is effectively increased. This is because more users are supported.

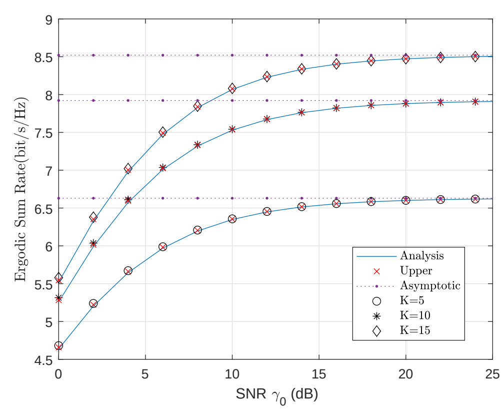

Fig. 9. The ESR of the system with different user numbers.

In Fig. 10 and Fig. 11, we plot the OP and ESR of RSMA-THz system with different antenna numbers over Nakagami fading channels (α=2), respectively, where N=16, 32, μ=2. From Fig. 10, it is found that the theoretical OP is consistent with the corresponding simulation, and the asymptotic OP can also match the simulation well at high SNR, which illustrates the accuracy of the presented theoretical OP analysis for

This article has been accepted for publication in a future issue of this journal, but has not been fully edited. Content may change prior to final publication.
Citation information: DOI 10.1109/JIOT.2025.3565925, IEEE Internet of Things Journal

the Nakagami channel. Moreover, the outage performance is effectively increased as the antenna number N increases. Besides, the system with APA scheme can obtain lower OP than that with the given FPA scheme, which further shows the effectiveness of the proposed PA scheme. As illustrated in Fig. 11, the theoretical ESR can agree well with the corresponding simulations, and the asymptotic ESR under high SNR region tends to a constant value at high SNR. Moreover, the upper bound of the ESR is slightly higher than the corresponding theoretical one. The above results shows that the presented theoretical rate analysis is accurate for Nakagami channel. Besides, the ESR is effectively increased with the increase of antenna number N, as expected.

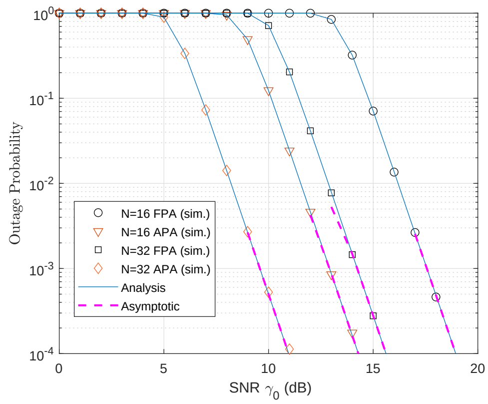

Fig. 10. The OP of the system with different antenna numbers.

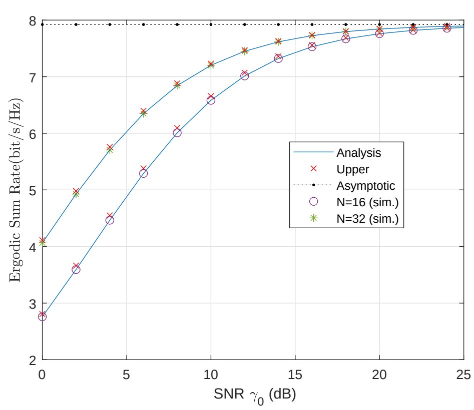

Fig. 11. The ESR of the system with different antenna numbers.

VI. Conclusion

The OP and the ESR of the multi-antenna RSMA-THz communication system with hardware impairment and imperfect SIC are investigated over composite fading channels, which considers the molecular absorption effect, misalignment fading and small-scale $\alpha-\mu$ fading in practice for the THz channel model. The closed-form PDF and CDF of effective channel gains are deduced for the performance analysis. Based on this, the closed-form expressions of OP are derived for performance evaluation and optimization. Also, the asymptotical OP of the system at high SNR is derived, and with this result, the system diversity gain is attained. By minimizing the OP subject to the constraint of sum power, the PA coefficients of common stream and private streams are designed, and the resultant closed-form PA scheme is obtained. With this PA scheme, the lower OP is attained. Thus, it provides an effective method to improve the outage performance of the RSMA-THz system.

Besides, to evaluate the rate performance of the system, the closed-form ESR expressions are deduced by means of the Fox-H and the Meijer-G functions. Considering the complexity of the theoretical ESR, the upper bound of ESR and its asymptotic expression are also derived to simplify the calculation of ESR. Furthermore, when α=2, which corresponds to small-scale Nakagami-m fading, the system ESR and its upper bound are also provided. Computer simulation shows that the theoretical analysis is consistent with the simulation result, which shows the accuracy of the theoretical derivation. The proposed PA scheme can obtain lower OP than the conventional fixed PA scheme. All the derived theoretical expressions can provide good performance evaluation for the RSMA-THz system, and avoid the conventional need for Monte Carlo simulation. Besides, the simulation results also assess the effects of the antenna number, misalignment fading parameter, small-scale fading, interference transfer factor and hardware impairments on the system performance. All these results will provide helpful guidelines for the system design.

Appendix A
Proof of Lemma 1

In this appendix, we give the proof of Lemma 1.

Proof: Let $g(x)=1+\frac{Ax}{Bx+1}, x\geq 0$, then $f(x)=\frac{\ln(g(x))}{\ln 2}$. Hence, we have:

$$f'(x)=\frac{1}{\ln 2}\frac{1}{g(x)}g'(x). \tag{65}$$

Since $A>0$, $B>0$, and $x\geq 0$, we can obtain that $g(x)\geq 1$ and $g'(x)=\frac{A}{(Bx+1)^2}>0$. Based on this, with (65), we have: $f'(x)>0$. Besides, $f''(x)$ can be expressed as

$$f''(x)=\frac{1}{\ln 2}\frac{g''(x)g(x)-g'(x)g'(x)}{g^2(x)}. \tag{66}$$

As $x\geq 0, g''(x)=\frac{-2AB}{(Bx+1)^3}<0$. Thus we have:

$$f''(x)=\frac{-2AB\left((A+B)x+1\right)-A^2}{(Bx+1)^4 g^2(x)\ln 2}<0. \tag{67}$$

Hence, $f(x)=\log_2\left(1+\frac{Ax}{Bx+1}\right)$ is a concave function. ■

Hence, Lemma 1 is proved.

Appendix B
Proof of Lemma 2

In this appendix, we give the proof of Lemma 2.

Proof: This can be proved by using the proof by contradiction. Let $\bar{k}=\underset{1\leq k\leq K}{\arg\min}\, b_k$ and $\hat{k}=\underset{1\leq k\leq K}{\arg\min}\, c_k$, then we have:

$$b_{\bar{k}}=\min b_k,\quad c_{\hat{k}}=\min c_k. \tag{68}$$

With (68), we can obtain that $b_{\hat{k}} \geq b_{\bar{k}} = \min b_k$. Based on this, if we assume that $\min b_k > \min c_k$, then we have: $c_{\hat{k}} < b_{\bar{k}} \leq b_{\hat{k}}$. However, this inequality contradicts the fact that $c_{\hat{k}} \geq b_{\hat{k}}$. Thus, the assumption does not hold. Hence, with the proof above, the Lemma 2 is proved. ■

ACKNOWLEDGMENTS

The authors would like to thank the anonymous reviewers for their valuable comments which improve the quality of this paper greatly.

REFERENCES

[1] J. Wang, C.-X. Wang, J. Huang, Y. Chen, "6G THz Propagation Channel Characteristics and Modeling: Recent Developments and Future Challenges," *IEEE Commun. Mag.*, vol. 62, no. 2, pp. 56-62, Feb. 2024.

[2] Y. Xu, Z. Liu, C. Huang, and C. Yuen, "Robust resource allocation algorithmforenergy-harvesting-based D2D communication underlaying UAV-assisted networks," *IEEE Internet Things J.*, vol. 8, no. 23, pp. 17161-17171, Dec. 2021.

[3] R. Deng, B. Di, H. Zhang, Y. Tan, and L. Song, "Reconfigurable holographic surface-enabled multi-user wireless communications: amplitude-controlled holographic beamforming," *IEEE Trans. Wireless Commun.*, vol. 21, no. 8, pp. 6003-6017, Aug. 2022.

[4] B. Sun, X. Yu, M. Chen, F. Jiang, Z. Zhu, and Z. Zheng, "Research on terahertz communication system and the prospect on space applications," *in Proc. IEEE Int. Conf. Adv. Infocomm Technol. (ICAIT)*, Hefei, China, Oct. 2023, pp. 67-72

[5] Y. Mao, O. Dizdar, B. Clerckx, R. Schober, P. Popovski, and H. V. Poor, "Rate-splitting multiple access: Fundamentals, survey, and future research trends," *IEEE Commun. Surv. Tutor.*, vol. 24, no. 4, pp. 2073-2126, Fourthquarter 2022.

[6] F. Xiao, X. Li, L. Yang, H. Liu and T. A. Tsiftsis, "Outage performance analysis of RSMA-aided semi-grant-free transmission systems," *IEEE Open J. Commun. Soc.*, vol. 4, pp. 253-268, 2023.

[7] J. Xu, O. Dizdar and B. Clerckx, "Rate-splitting multiple access for short-packet uplink communications: A finite blocklength analysis," *IEEE Commun. Lett.*, vol. 27, no. 2, pp. 517-521, Feb. 2023.

[8] H. Lei, S. Zhou, K.-H. Park, I. S. Ansari, H. Tang, and M.-S. Alouini, "Outage analysis of millimeter wave RSMA systems," *IEEE Trans. Commun.*, vol. 71, no. 3, pp. 1504-1520, 2023.

[9] O. S. Badarneh, M. T. Dabiri and M. Hasna, "Channel modeling and performance analysis of directional THz links under pointing errors and α-μ distribution," *IEEE Commun. Lett.*, vol. 27, no. 3, pp. 812-816, Mar. 2023.

[10] P. Bhardwaj and S. M. Zafaruddin, "Exact performance analysis of THz link under transceiver hardware impairments," *IEEE Commun. Lett.*, vol. 27, no. 8, pp. 2197-2201, 2023.

[11] E. N. Papasotiriou, A. -A. A. Boulogeorgos and A. Alexiou, "Performance analysis of THz wireless systems in the presence of antenna misalignment and phase noise," *IEEE Commun. Lett.*, vol. 24, no. 6, pp. 1211-1215, Jun. 2020.

[12] O. S. Badarneh, "Performance analysis of terahertz communications in random fog conditions with misalignment," *IEEE Wireless Commun. Lett.*, vol. 11, no. 5, pp. 962-966, May 2022.

[13] K. Guan, D. He, B. Ai, Y. Chen, C. Han, B. Peng, Z. Zhong, T. Krner., "Channel characterization and capacity analysis for THz communication enabled smart rail mobility," *IEEE Trans. Veh. Technol.*, vol. 70, no. 5, pp. 4065-4080, May 2021.

[14] S. Li, L. Yang, J. Zhang, P. S. Bithas, T. A. Tsiftsis and M.-S. Alouini, "Mixed THz/FSO relaying systems: Statistical analysis and performance evaluation," *IEEE Trans. Wireless Commun.*, vol. 21, no. 12, pp. 10996-11010, Dec. 2022.

[15] S. Li and L. Yang, "Performance analysis of dual-hop THz transmission systems over α-μ fading channels with pointing errors," *IEEE Internet Things J.*, vol. 9, no. 14, pp. 11772-11783, Jul. 2022.

[16] P. Bhardwaj, V. Bansal, N. Biyani, S. Shukla, and S. M. Zafaruddin, "Performance of integrated IoT network with hybrid mmWave/FSO/THz backhaul link," *IEEE Internet Things J.*, vol. 11, no. 12, pp. 3639-3652, Jau. 2024.

[17] Y. Yin, L. Yang, X. Li, H. Liu, K. Guo and Y. Li, "On the performance of active RIS-assisted mixed RF-THz relaying systems," *IEEE Internet Things J.*, early access, 2025.

[18] T. H. Vu, Q. V. Pham, and S. Kim, "On performance of downlink THz-based rate-splitting multiple-access (RSMA): is it always better than NOMA?," *IEEE Trans. Veh. Technol.*, vol. 73, no.3, pp. 4435-4440, 2024.

[19] X. Chen, F. Yan, M. Hu, and Z. Lin, "Energy efficiency optimization of intelligent reflective surface-assisted terahertz-RSMA system," in *Proc. 2023 28th Asia Pacific Conference on Communications (APCC)*, Nov.19-22, 2023, pp.307-312.

[20] X. Su, K. Xu, Y. Xu, and W. Ma, "Multipair two-way massive mimo af relaying with zfr/zft and hardware impairments over high-altitude platforms,"*J. Commun. Inf. Netw.*, vol. 1, no. 3, pp. 105-114, Oct. 2016.

[21] Y. Zhang, M. Zhou, H. Zhao, L. Yang, and H. Zhu, "Spectral efficiency of superimposed pilots in cell-free massive mimo systems with hardware impairments,"*China Commun.*, vol. 18, no. 6, pp. 146-161, Jun. 2021.

[22] Z. Xiang, X. Tong, Y. Cai, "Secure transmission for NOMA systems with imperfect SIC" *China Commun.*, vol. 17, no. 11, pp. 67-78, 2020.

[23] Z. Xiang, W. Yang, G. Pan, Y. Cai, Y. Song, and Y. Zou, "Secure transmission in HARQ-assisted non-orthogonal multiple access networks," *IEEE Trans. Inf. Forensics Security*, vol. 15, pp. 2171-2182, 2020.

[24] P. K. Singya, B. Makki, A. DErrico, and M.-S. Alouini, "Hybrid FSO/THz-based backhaul network for mmWave terrestrial communication," *IEEE Trans. Wireless Commun.*, vol. 22, no. 7, pp. 4342-4359, 2023.

[25] E. N. Papasotiriou, A.-A. A. Boulogeorgos, K. Haneda, M. F. de Guzman, and A. Alexiou, "An experimentally validated fading model for THz wireless systems" *Sci. Rep.*, vol. 11, no. 1, pp. 1C14, Sep. 2021.

[26] D. B. da Costa, M. D. Yacoub, and J. C. S. S. Filho, " Highly accurate closed-form approximations to the sum of α-μ variates and applications,"*IEEE Trans. Wireless Commun.*, vol. 7, no. 9, pp. 4342-4359, 2008.

[27] M. D. Yacoub, "The α-μ distribution: a physical fading model for the stacy distribution," *IEEE Trans. Veh. Technol.*, vol. 56, no. 1, pp. 27-34, 2007.

[28] A. A. Farid and S. Hranilovic,"Outage capacity optimization for free-space optical links with pointing errors" *J. Lightw. Technol.*, vol. 25, no. 7, pp. 1702-1710, Jul. 2007.

[29] I. S. Gradshteyn and I. M. Ryzhik, *Table of integrals, series, and products*. Academic press, 2007.

[30] P. Bhardwaj and S. M. Zafaruddin, "Performance of dual-hop relaying for THz-RF wireless link over asymmetrical α-μ fading," *IEEE Trans. Veh. Technol.*, vol. 70, no. 10, pp. 10031-10047, 2021.

[31] S. K. Singh, K. Agrawal, K. Singh, and C.-P. Li, "Ergodic capacity and placement optimization for RSMA-enabled UAV-assisted communication," *IEEE Systems J.*, vol. 17, no. 2, pp. 2586-2589, 2022.

[32] Y. Mao, E. Piovano, and B. Clerckx, "Rate-splitting multiple access for overloaded cellular internet of things," *IEEE Trans. Commun.*, vol. 69, no. 7, pp. 4504-4519, 2021.

[33] Z. Rahman, M. Z. Hassan, and G. Kaddoum, "Ergodic capacity optimization for RSMA-Based UOWC systems over EGG turbulence channel," *IEEE Commun. Lett.*, 2024.

[34] S. K. Singh, K. Agrawal, K. Singh, and C.-P. Li, "Ergodic capacity and placement optimization for RSMA-enabled UAV-assisted communication," *IEEE Systems J.*, vol. 17, no. 2, pp. 2586-2589, 2022.

[35] V. S. Adamchik and O. Marichev, "The algorithm for calculating integrals of hypergeometric type functions and its realization in REDUCE system," in *Proceedings of the international symposium on Symbolic and algebraic computation*, 1990, pp. 212-224.

[36] *The wolfram functions site*, http://functions.wolfram.com/07.34.21.0012.01, Visited on Aug.1,2023.

[37] A. M. Mathai, R. K. Saxena, and H. J. Haubold, *The H-function: theory and applications*. Springer Science & Business Media, 2010.

[38] S. G. Krantz, *Handbook of complex variables*. Springer Science & Business Media, 1998.